Design and Multi-Objective Optimization of EMI Input Filters

Nico Hensgens, Jesus Oliver, Jose A. Cobos Stanislav Skibin, Andreas Ecklebe

I. Introduction

In order to comply with international conducted electromagnetic interference (EMI) standards, power converters generally require an EMI input filter. Normally this filter can only be designed efficiently once the input current spectrum of the converter is available, through measurements on a converter prototype. In practice the filter performance strongly depends on a proper impedance mismatch between the filter output impedance and the converter high-frequency input impedance, or noise source impedance, which also needs to be measured on a working converter prototype. Therefore, the EMI filter design is traditionally performed as one of the last steps in converter design and prototyping. Additionally, high-frequency parasitic effects of the filter components, if not considered during the filter design, lead to increasingly large differences between the calculated filter performance and the real filter performance at high frequencies. This often leads to sub-optimal designs and several design iterations until an adequate filter design has been found.

In order to reduce the design time and cost and obtain optimal filter designs, a filter design procedure is required which takes into consideration all above mentioned effects, i.e. noise spectrum, converter noise source impedance and high-frequency parasitic effects. The design procedure should be based on detailed component models and employ multi-objective optimization techniques to obtain optimal designs with respect to a specific performance function, considering e.g. filter performance, weight, volume, cost, etc.

II. Analytical Filter Description

ABCD network parameters are used for an analytical description of the input filters. Network parameters allow easy calculation of all important filter parameters, such as input impedance, output impedance and attenuations [5]. The network parameters of cascaded filter elements, i.e. series inductances and shunt capacitances, can be obtained by simple multiplication of the parameter matrices of the individual elements. A single-phase filter can be described by a four-port network and the DM and CM equivalent circuits can be described by two two-port networks which can be easily obtained from the four-port network. The different networks of a single stage filter are shown in Fig.14 and their mathematical descriptions are given in (1)-(3) respectively.

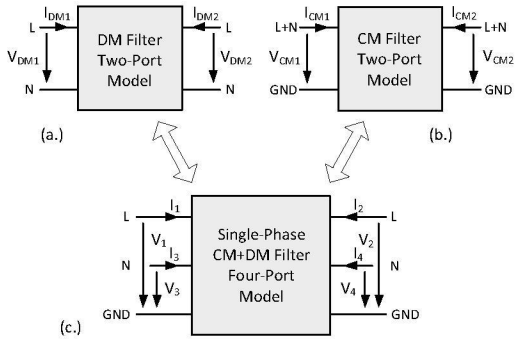

Fig. 1. Four-port network used for analytical description of a single-phase EMI filter (c.), DM equivalent two-port network (b.), CM equivalent two-port network (a.).

$$\begin{pmatrix} V_2 \\ I_2 \\ V_4 \\ I_4 \end{pmatrix} = \begin{pmatrix} a_{11} & a_{12} & a_{13} & a_{14} \\ a_{21} & a_{22} & a_{23} & a_{24} \\ a_{31} & a_{32} & a_{33} & a_{34} \\ a_{41} & a_{42} & a_{43} & a_{44} \end{pmatrix} \begin{pmatrix} V_1 \\ -I_1 \\ V_3 \\ -I_3 \end{pmatrix} \quad (1)$$

$$\begin{pmatrix} V_{DM2} \\ I_{DM2} \end{pmatrix} = \begin{pmatrix} d_{11} & d_{12} \\ d_{21} & d_{22} \end{pmatrix} \begin{pmatrix} V_{DM1} \\ -I_{DM1} \end{pmatrix} \quad (2)$$

$$\begin{pmatrix} V_{CM2} \\ I_{CM2} \end{pmatrix} = \begin{pmatrix} c_{11} & c_{12} \\ c_{21} & c_{22} \end{pmatrix} \begin{pmatrix} V_{CM1} \\ -I_{CM1} \end{pmatrix} \quad (3)$$

In case of a three-phase filter, a six-port network is necessary, which can be split into three individual DM two-port networks

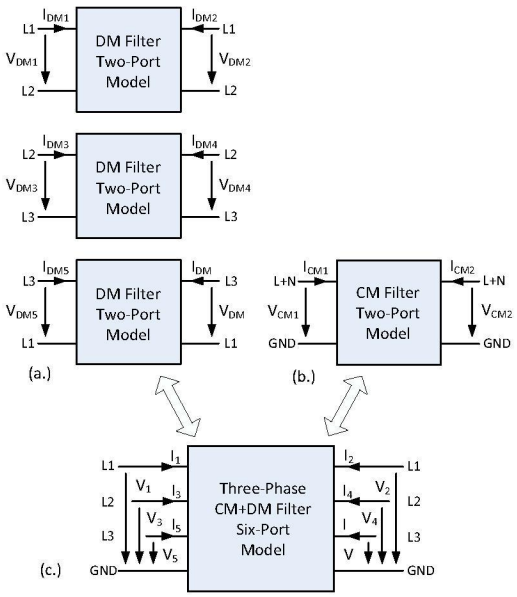

Fig. 2. Six-port network used for analytical description of a three-phase EMI filter (c.), DM equivalent two-port networks (b.), CM equivalent two-port network (a.).

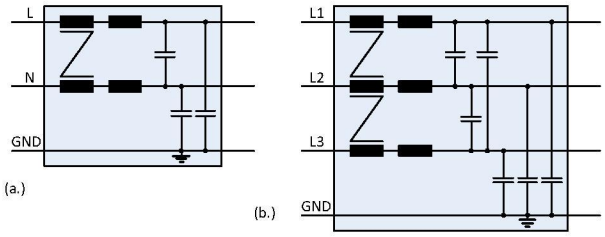

Fig. 3. Exemplary filters depicted as multi-port networks: (a.) single-phase 2^{nd} order LC CM and DM filter as a four-port network, (b.) three-phase 2^{nd} order LC CM and DM filter as a six-port network.

(which should however be identical in case of a symmetrical system) and one CM two-port network. This is shown in Fig.2. The expressions for the three-phase networks as well as the transformations are not provided due to space constraints.

III. Noise Impedance Measurement and Filter Topology Selection

It is a well known fact that in order to obtain an optimal filter performance, the output impedance of the filter and the noise source impedance of the converter, as well as the input impedance of the filter and the load impedance of the filter need to be properly mismatched. These quantities are defined in Fig.4. In practice, i.e. in conducted EMI measurements according to [1], [2], the filter load impedance is well defined by the line-impedance stabilization network (LISN) and the

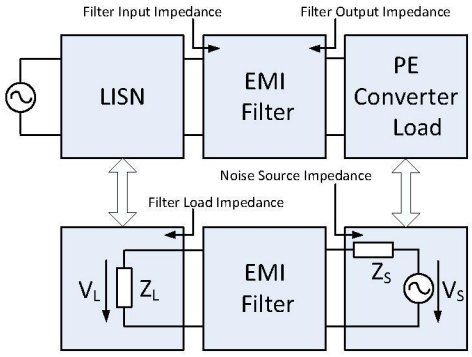

Fig. 4. Definition of filter load impedance, input and output impedances and noise source impedance.

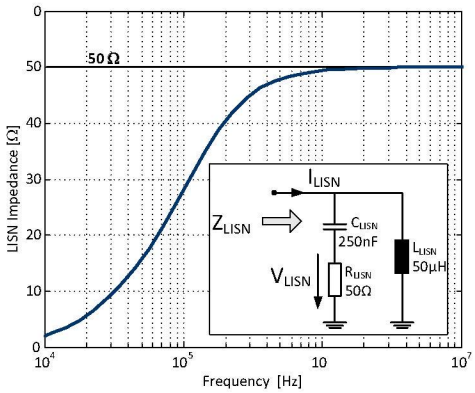

Fig. 5. Simplified LISN impedance network and impedance profile.

source impedance is the DM or CM noise source impedance of the converter system as shown in Fig.4.

A. Load Impedance

As already stated the filter load impedance is given by the LISN and is equal to 50Ω at high frequencies. A simplified LISN schematic which is valid for high frequencies and the related impedance profile are shown in Fig.5

B. Source Impedance

The power converter can be modeled for both CM and DM conducted EMI as a voltage source $V_{S,CM}$ or $V_{S,DM}$, together with a CM or DM noise source impedance $Z_{L,CM}$ or $Z_{L,DM}$ [9]. In order to measure the noise source impedances of a converter, different methods have been presented in the literature, which are: the resonance method [13], the insertion loss method [14], the two current probes approach [15], and most recently, the direct-clamped two current probes approach [16]. In the two current probes approaches, an injecting current probe and a receiving current probe are used together with a vector network analyzer, to identify the unknown source impedance under operating conditions.The basic principle of

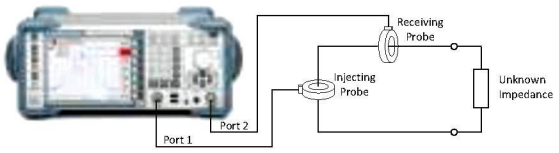

Fig. 6. Two current probes approach to measure noise source impedances.

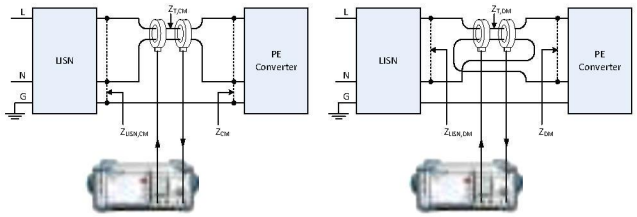

Fig. 7. Direct-clamped two current probes approach to measure the CM (left) and DM (right) noise source impedance of a power electronic converter under operating conditions.

operation is shown in Fig.6. In the method presented in [16] the two current probes are directly clamped to the converter input port to obtain both the CM and DM noise source impedance of the converter system. The two ways of connecting the probes for DM and CM impedance measurements are shown in Fig.7(a.) and Fig.7(b.) respectively. Details on how the noise source impedances can be identified using these measurements can be found in [16].

C. Effect of Impedance Mismatch

To obtain an analytical description of the effect an improper impedance mismatch has on the filter performance, we consider the system in Fig.8. This system consists of a filter described using a two-port network (which can be a DM or CM model of any filter) together with its load impedance Z_L (defined by the LISN) and a model of the converter containing an equivalent (CM or DM) noise source V_S and (CM or DM) noise source impedance Z_S. The two-port network shall have the following description

$$\begin{pmatrix} V_2 \\ I_2 \end{pmatrix} = \begin{pmatrix} A_{11} & A_{12} \\ A_{21} & A_{22} \end{pmatrix} \begin{pmatrix} V_1 \\ -I_1 \end{pmatrix} \tag{4}$$

We are interested in the transfer function $T(\omega) = \frac{V_L}{V_T}$. From

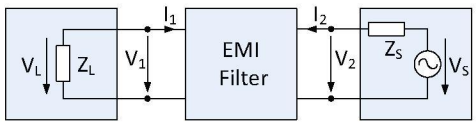

Fig. 8. Two-port equivalent network of a CM or DM EMI filter with load impedance and converter CM or DM noise equivalent circuit, consisting of equivalent noise source and noise source impedance.

the system in Fig.8 and (4) we can obtain the following expression:

$$T(\omega) = \frac{V_L}{V_S} = \frac{1}{A_{11} + A_{12}\frac{1}{Z_L} + A_{21}Z_S + A_{22}\frac{Z_S}{Z_L}} \tag{5}$$

Based on this equation it is possible to estimate the attenuation provided by the filter connected to load and source impedances Z_L and Z_S. In the case where only ideal filter elements without parasitics are assumed, (5) can be approximated using [10]:

$$\tilde{T}(\omega) = \frac{1}{\omega^p \prod_{i=1}^{p} L^i \cdot \omega^q \prod_{j=1}^{q} C^j} \frac{Z_S + Z_L}{Z_L} \cdot K \tag{6}$$

with

$$K = \begin{cases} 1 & = \textit{ for LC-type filters} \\ \frac{Z_L}{Z_S} & = \textit{ for CL-type filters} \\ Z_L & = \textit{ for LCL-type filters} \\ \frac{1}{Z_S} & = \textit{ for CLC-type filters} \end{cases} \tag{7}$$

As an example the attenuation characteristics $T(\omega)$ of a fourth-order filter (both $LCLC$ and $CLCL$ topologies are considered) under different source impedance conditions are shown in Fig.9. The load impedance is set to 50Ω (approximation of LISN impedance) in all cases and the noise source impedance is considered to be either purely inductive or purely capacitive. One can see that in case of a proper impedance mismatch, i.e. inductive filter output-impedance vs. capacitive noise source impedance, or vice-versa, the calculated attenuation (solid green line) matches the ideal attenuation (dotted black line) (cf. Fig.9(b.) and Fig.9(c.)). However when there is an improper impedance mismatch, i.e. when the filter output impedance and the noise source impedance are both inductive or both capacitive, the filter performance degrades by a factor of $20dB/decade$ (cf. Fig.9(a.) and Fig.9(d.)).

D. Filter Topology Selection

In case of a proper impedance mismatch a maximal rejection of the noise currents is obtained which are prevented from flowing from the power supply into the power grid. This fact leads to a rule for the filter topology selection which in its simplest case can be tranlslated into a selection map as shown in Fig.10. This table shows, for the example of 2^{nd} and 3^{rd} order filters, the topology which should be selected depending on the source and load impedance to which the filter will be connected. This selection criterion can immediately be extended to higher order filter topologies. Once the filter input and ouput components have been chosen according to Fig.10, the number of filter stages needs to be selected depending on the attenuation requirements. The required attenuation can be obtained from the input current spectra of the converter (ideally both the CM and DM current spectrum should be available separately) and the applicable conducted EMI standard limits. A generic noise spectrum together with the conducted EMI limits as defined in [1] and [2] is shown in Fig.11. The required attenuation can simply be obtained by subtracting the noise limit from the current spectrum. To be on the safe side during filter design an additional tolerance

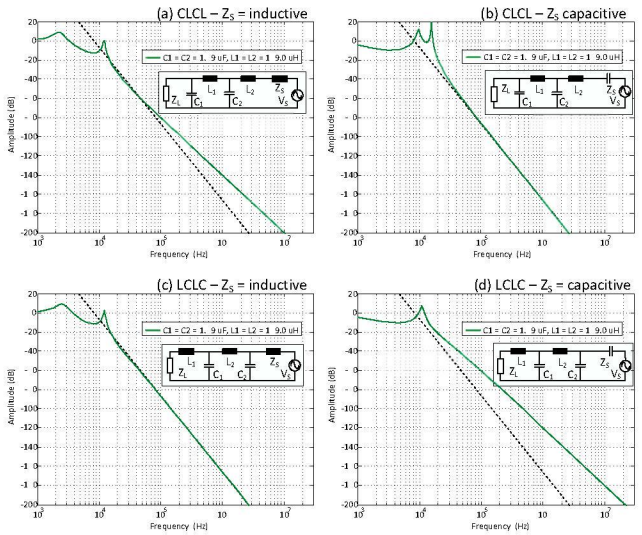

Fig. 9. Effect of noise source impedance mismatch on the filter performance of 4^{th} order filters. (a.) CLCL filter with inductive source impedance, (b.) CLCL filter with capacitive source impedance, (c.) LCLC-filter with inductive source impedance, (d.) LCLC-filter with capacitive source impedance. Calculated attenuation profiles are in green, the black lines denote HF approximations in case of ideal impedance mismatch.

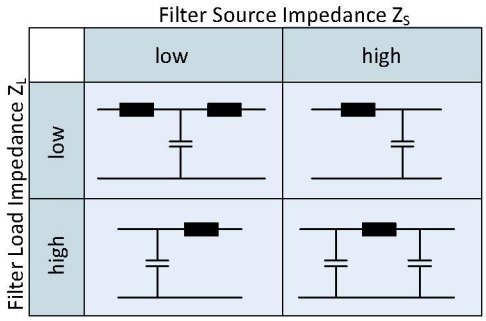

Fig. 10. Table of impedance mismatch conditions which should be met by filter to obtain good filter performance. Filters of 2^{nd} and 3^{rd} order are shown, the table can however be generalized to filter with different order.

margin of several $dB\mu V$ should be added which then provides the filter attenuation, the EMI filter is supposed to provide. This is depicted graphically in the upper part of Fig.12 using a simplified noise spectrum and noise limit. In many cases the filter topology selection and design is simply based on the first high noise peak in the frequency range of interest, i.e. $150kHz - 30MHz$, which normally coincides with the first switching frequency harmonic lying in this range. In that case it is assumed that, since the attenuation of an n-th order filter increases with $n \cdot 20dB\mu V$ per frequency decade, when the filter provides enough attenuation for this first noise peak, all other noise peaks are also taken care of. However if the topology selection has to be performed automatically and in case of a more complicated noise spectrum like the one shown

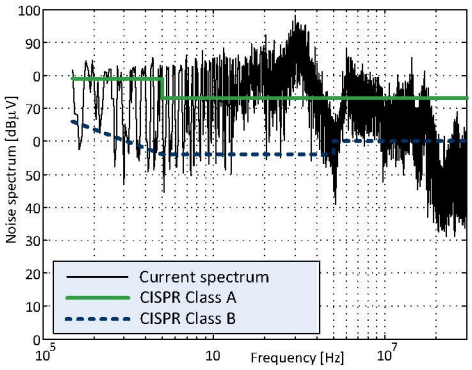

Fig. 11. Generic converter conducted EMI spectrum (black) and CISPR class A (solid green) and class B (dotted blue) conducted emission standard limits

in Fig.11, identification of the required attenuation using this first noise peak is not allways possible. The simplified noise spectrum in the upper part of Fig.12 consists of two noise peaks at frequencies f_{n1} and f_{n2} with amplitudes A_{n1} and A_{n2} respectively. By subtracting the noise limit and adding an additional margin, we obtain the required attenuation profile shown in the bottom part of Fig.12 consisting of the same two peaks at frequencies f_{n1} and f_{n2} and with amplitudes A_{f1} and A_{f2}. If now only the first peak with amplitude A_{f1} is considered for designing the filter, a filter providing a slope s_1 of e.g. $-40dB\mu V/decade$ and cutoff frequency f_{c2} might appear sufficient. However as can be seen, this filter does not provide enough attenuation to damp the second noise peak. Thus in case of this filter topology the second noise peak turns out to be more critical than the first one, and maintaining the same filter topology a larger filter with cutoff frequency f_{c1} would be necessary to provide enough attenuation for both noise peaks. However in case another filter topology with higher order and a slope s_2 of e.g. $-80dB\mu V/decade$ is selected and designed based on the first noise peak, also the second noise peak is sufficently attenuated (cf. Fig.12). A conclusion is that in case the filter topology is to be selected automatically based on the required attenuation profile, the complete spectrum with all major noise peaks needs to be considered since the most critical noise peak for the dimensioning of the filter depends on the selected filter topology.

IV. Multi-Objective Optimization Framework

A multi-objective optimization approach is employed to obtain filters which are optimal with respect to some previously defined performance function. The optimization framework [6] consists of two spaces, one design space and one performance space as well as a mapping function and an optimization algorithm as depicted in Fig.13. The design space is spanned by the values of the individual filter components x_i. The performance space is spanned by a set of performance indices p_i. The mapping function maps each point in the design space,

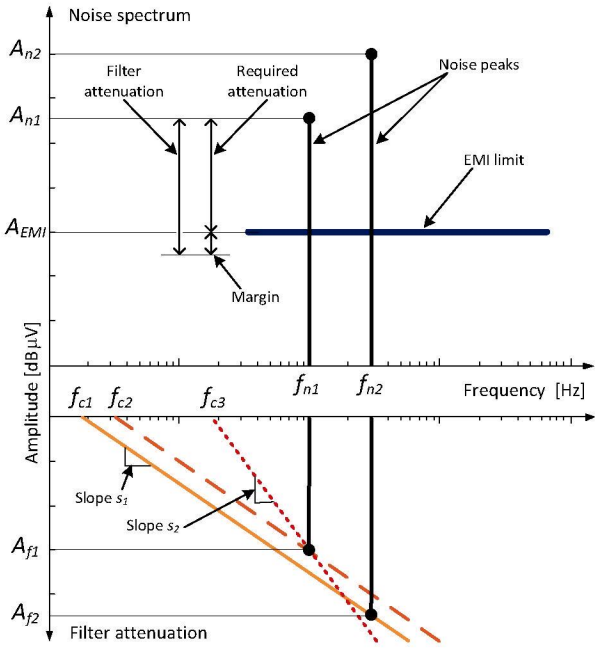

Fig. 12. Simplified noise spectrum consisting of two peaks with different amplitudes (top), required filter attenuation and attenuation achieved of filters with different slopes and cutoff frequencies (bottom).

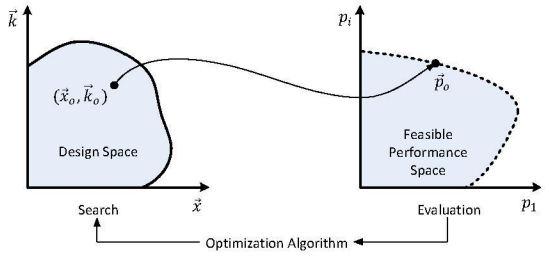

Fig. 13. Graphical depiction of optimization framework [6].

defining one possible filter configuration, into the performance space. The performance space allows an objective evaluation and comparison of different filter designs. An optimization algorithm can then be used to efficiently find a point in the design space with optimal perormance characteristics.

V. Design Space Analysis and Mapping

A. Design Space Definition

The design space is spanned by the n individual filter elements, i.e. the series inductors and shunt capacitors. Thus the number of dimensions of the design space equals the number of filter elements or the order of the filter. If a filter of order n, providing a given attenuation att (given in $dB\mu V$) at a frequency f_{att} needs to be designed, the product X of all

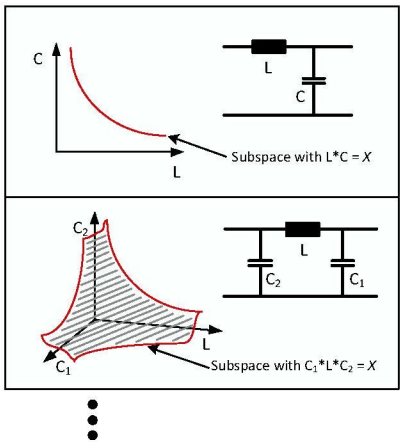

Fig. 14. Graphical depiction of the design spaces for filters of order 2 and 3. The number of dimensions of the design space coincides with the order of the filter, i.e. the number of reactive filter elements.

n filter components can be calculated as:

$$X = \frac{10^{\frac{att}{20}}}{(2\pi f_{att})^n} \tag{8}$$

All component combinations equaling this specific value X form a sub-space of dimension $n-1$ in the n-dimensional design space. This is depicted graphically in Fig.14 for filters of second and third order.

B. Design Constraints

Additional requirements for the filter are used to provide constraints in the design space, e.g. converter stability considerations normally lead to a minimal source impedance for the converter which translates into a minimal value of the filter output capacitance [12] or restrictions on the reactive energy in the filter components lead to a maximal value of all filter capacitors [11].

C. Component Models and Inductor Design

The mapping from the design space to the performance space is achieved through the selection and design of the individual filter components. To perform this task, databases of commercially available filter capacitors and toroidal cores have been created. The capacitor database contains information on the component values, including high-frequency parasitic elements such as equivalent series inductance (ESL) and equivalent series resistance (ESR), as well as component volume (width, length and height) and weight. Typical EMI filter capacitors used in CM and DM filters are shown in Fig.15, together with their idealized and more detailed HF-models. Whereas the filter capacitors are readily commercially available, the filter inductors need to be designed. Databases of powder and ferrite cores with toroidal geometry [18], [19] have been created, as well as of some commercially available filter chokes [20]. The databases include weight and volume

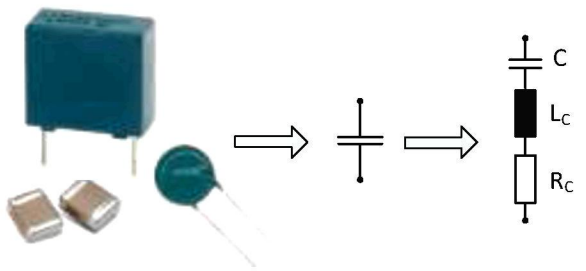

Fig. 15. DM and CM, film and ceramic EMI filter capacitors: components (left), component symbol (center) and component model including high-frequency parasitics (right)

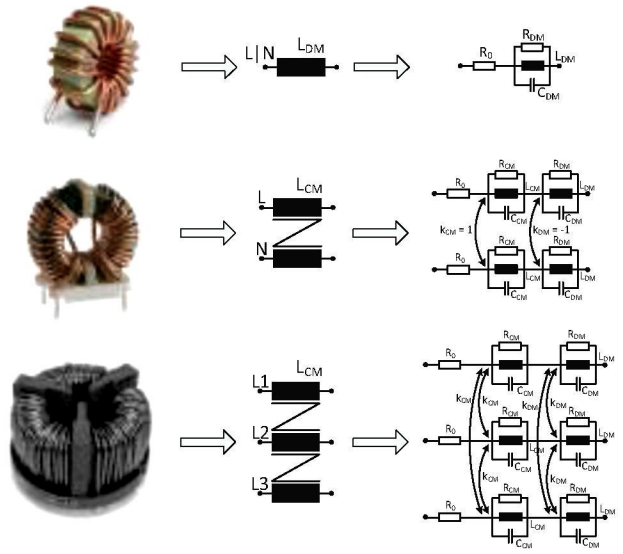

Fig. 16. Differential mode (top), DC or single-phase common mode (middle) and three-phase common-mode (bottom) chokes for EMI filter applications, component (left, components symbol (center) and component model including high-frequency parasitics (right) [17]

information of the cores as well as material properties, e.g. permeability. The inductance of a toroidal inductor as shown in Fig.17 is given by:

$$L = N^2 \mu_r \mu_0 \frac{A_e}{l_e} \tag{9}$$

The material properties $\mu_r \mu_0$ and geometrical properties l_e and A_e can be summarized for each core in the so called A_L-value and which is in case of many toroidal cores provided by the manufacturer. The initial number of turns to obtain an inductance L using a core with a specifc A_L can than be calculated using:

$$N = \sqrt{\frac{L}{A_L}} \tag{10}$$

In a next step the magnetic field and the resulting magnetic

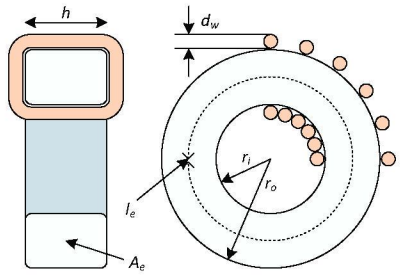

Fig. 17. Schematic of a toridal core with windings employed in EMI input filters.

flux inside the core need to be calculated, this can be done using the magnetization curves or analytically using (11) and the set of curve fitting parameters (a, b, c, d, e, x) provided by the manufacturers. The core should not be driven into saturation, even at the peak value of the low frequency AC input current.

$$B = \left(\frac{a + bH + cH^2}{1 + dH + eH^2} \right)^x \tag{11}$$

In a next step the total losses of the inductor need to be calculated, which consist of conduction losses in the wire and core losses. Both loss components can be split in a low-frequency and a high-frequency part. Details on the loss calculations can be found e.g. in [21], [22]. The total power losses lead to a temperature rise ΔT and a resulting change in the permeability, leading to a new inductance value and the necessity of an adaptation in the number of turns. According to [18] and [22] the temperature rise can be estimated using:

$$\Delta T = \left(\frac{\textit{total power loss}}{\textit{surface area}} \right)^{0.833}, \tag{12}$$

and the resulting change in permeability is given by:

$$\Delta \mu(T) = a + bT + cT^2 + dT^3 + eT^4 \quad [\%], \tag{13}$$

again using curve fitting coefficients provided by the manufacturer. This design approach is used iteratively until a steady-state in temperature, permeability and number of turns is reached. Then the total losses of the inductor have already been calcualted and the resulting weight can be calculated as the sum of the weight of the core and the wire.

VI. Performance Space Analysis

In order to objectively analyze and compare the performance of different filters, a set of performance metrics, especially adapted for the characterization of EMI filters, is proposed. In order to define the metrics, first two auxiliary quantities are defined; these are the *ideal attenuation area* and the *real attenuation area*. These two quantitities describe the area formed by the attenuation profile of a given filter in the frequency range defined by the conducted EMI standards, i.e. $150kHz$ - $30MHz$. In the ideal attenuation area the theoretical

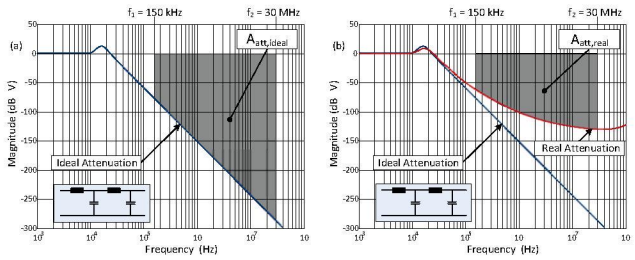

Fig. 18. Definition of ideal attenuation area and real attenuation area

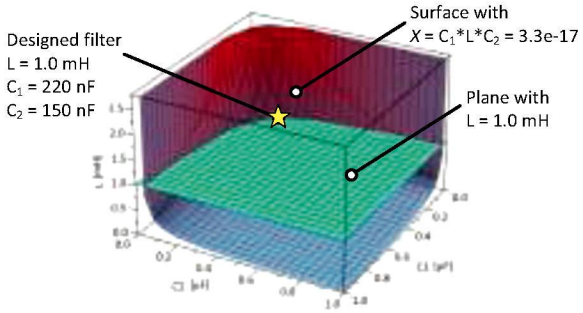

Fig. 19. Design space of a third order CLC filter, the purple surface contains all possible component combinations with $X = C_1 \cdot L \cdot C_2 = 3.4 * 10^{-17}$

characteristics of an ideal filter are considered whereas in the real attenuation area, the characteristics of a real filter are considered. The two quantities are defined in (14) and (15) and depicted graphically in Fig.18 for the example of a fourth order filter.

$$A_{att,ideal} = \left| \int_{log(f_1)}^{log(f_2)} T_{ideal}(f) dlog(f) \right| \tag{14}$$

$$A_{att,real} = \left| \int_{log(f_1)}^{log(f_2)} T_{real}(f) dlog(f) \right| \tag{15}$$

Based on these quantitites the following five performance metrics are defined:

- Efficiency:

$$\eta = \frac{P_{out}}{P_{in}} = 1 - \frac{P_{loss}}{P_{in}} \tag{16}$$

- Attenuation performance:

$$\chi = \frac{A_{att,real}}{A_{att,ideal}} \tag{17}$$

- Power·attenuation/weight

$$\gamma = \frac{P_{in} \cdot A_{att,ideal}}{Weight} \quad \left[\frac{W \cdot dB\mu V \cdot log(Hz)}{kg} \right] \tag{18}$$

- Power·attenuation/volume

$$\rho = \frac{P_{in} \cdot A_{att,ideal}}{Volume} \quad \left[\frac{W \cdot dB\mu V \cdot log(Hz)}{l} \right] \tag{19}$$

- Power·attenuation/cost

$$\sigma = \frac{P_{in} \cdot A_{att,ideal}}{Cost} \quad \left[\frac{W \cdot dB\mu V \cdot log(Hz)}{\$} \right] \tag{20}$$

VII. Design Example

An example DM filter providing an attenuation of $60 dB\mu V$ at a frequency of $500 kHz$ has been designed. A third order filter with a CLC topology has been selected. The design space of this filter is shown in Fig.19. From the design space in Fig.19, the following component values have been selected: $C_1 = 220nF$, $L = 1mH$ and $C_2 = 150nF$. The capacitor values are commercially available and can be immediately selected. The inductor however needs to be designed. In order to find a choke with a good tradeoff between weight and losses, an exhaustive search of possible designs based on the core

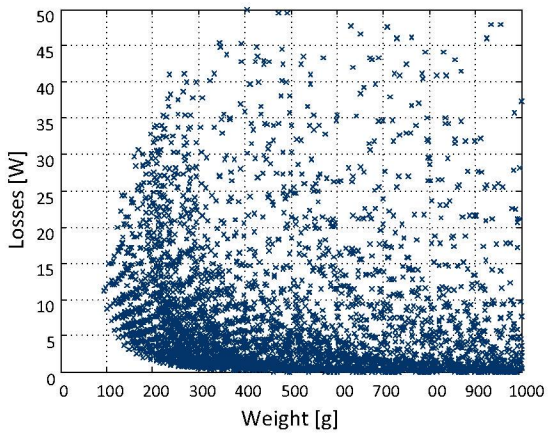

Fig. 20. Simplified performance space with the filter weight and losses as performance indices.

database and available wire diameters has been performed. The results are shown in Fig.20. Here a pareto-front appears which gives all designs with optimal tradeoffs between minimal losses and weight. Fig.21 shows different attenuation curves of this filter: the dashed-blue curve shows the attenuation in case ideal components are assumed, as shown in Fig.22(a.), the solid-green curve shows the calculated attenuation in case component models with parasitic elements are assumed, as shown in Fig.22(b.), and the dotted red line shows the actual filter performance, in case all parasitic elements, including interconnect parasitics and mutual couplings between the components are econsiderd, as shown in Fig.22(c.). From this design example it becomes clear that the performance of the real filter is far worse at high frequencies than the calculated performance in case ideal components are assumed, or even if components including parasitic elements are considered. Due to this fact the use of the proposed performance metrics is still limited. More detailed filter models including interconnect parasitics need to be employed to obtain more accurate estimations of the filter performance during the design and

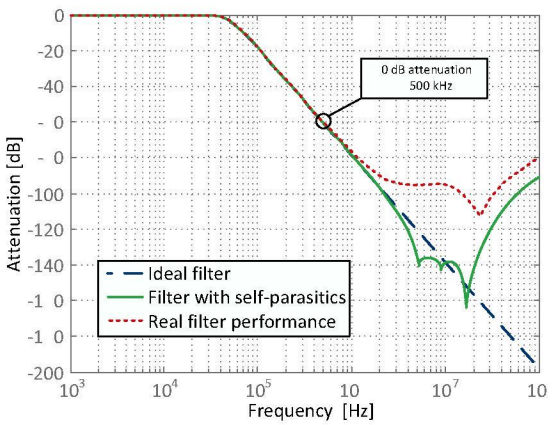

Fig. 21. Filter attenuation of the ideal CLC filter (dashed-blue), including parasitic elements (solid-green) and the real filter (dotted-red).

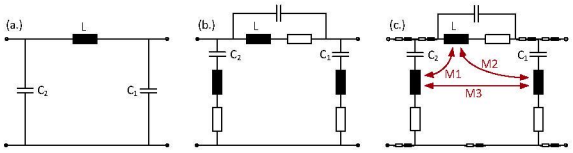

Fig. 22. Differenmt models of the considered third order CLC filter considering only (a.) only ideal elements, (b.) components with parasitics and (c.) components with parasitics, interconnect parasitics and mutual component couplings.

optimization process. In that case the approach using analytical filter descriptions as employed in this work will be limited, due to the high complexity of interconnect parasitics models. In this case fast numerical simulation models should be employed to characterize the filter during the optimization procedure.

VIII. Conclusion

A filter design methodology has been presented, based on selection of filter topologies for proper impedance mismatch between the filter output and the converter noise source impedances, databases of filter components and optimization of the individual filter components. The filter design procedure is embedded into a multi-objective optimization framework, which allows fast identification of optimal designs with respect to a specific cost function. The general methodology has been described, employing a topology-dependent design space and a performance space which allows comparison of different filter designs based on a set of performance metrics, specifically defined for characterization of EMI input filters.
Future steps will include the consideration of interconnect parasitics in the filter design, in which case the approach employing analytical filter descriptions needs to be replaced by numerical simulation models.

Acknowledgment

The authors would like to thank ABB Switzerland Ltd. for funding and scientific support of this project.